Photochemistry and Photobiology, 2022, 98: 334–346

Special Issue Research Article

Caged Oxime Reactivators Designed for the Light Control of Acetylcholinesterase Reactivation†

Jayme Cannon[1,2], Shengzhuang Tang[1,2] and Seok Ki Choi[1,2]*

[1]Michigan Nanotechnology Institute for Medicine and Biological Sciences, University of Michigan Medical School, Ann Arbor, Michigan, USA
[2]Department of Internal Medicine, University of Michigan Medical School, Ann Arbor, Michigan, USA

Received 16 August 2021, revised 17 September 2021, accepted 22 September 2021, DOI: 10.1111/php.13530

ABSTRACT

Despite its promising role in the active control of biological functions by light, photocaging remains untested in acetylcholinesterase (AChE), a key enzyme in the cholinergic family. Here, we describe synthesis, photochemical properties and biochemical activities of two caged oxime compounds applied in the photocontrolled reactivation of the AChE inactivated by reactive organophosphate. Each of these consists of a photocleavable coumarin cage tethered to a known oxime reactivator for AChE that belongs in an either 2-(hydroxyimino)acetamide or pyridiniumaldoxime class. Of these, the first caged compound was able to successfully go through oxime uncaging upon irradiation at long-wavelength ultraviolet light (365 nm) or visible light (420 nm). It was further evaluated in AChE assays *in vitro* under variable light conditions to define its activity in the photocontrolled reactivation of paraoxon-inactivated AChE. This assay result showed its lack of activity in the dark but its induction of activity under light conditions only. In summary, this article reports a first class of light-activatable modulators for AChE and it offers assay methods and novel insights that help to achieve an effective design of caged compounds in the enzyme control.

Abbreviations: AChE, acetylcholinesterase; DEACM, 6-(diethylamino)coumarin-4-methyl; OP, reactive organophosphate; POX, paraoxon.

INTRODUCTION

Development of light-controlled strategies has made a remarkable impact on recent advances in many areas from chemical biology (1–4), pharmacology (5–7) to drug delivery (8–11). In particular, the strategy of photocaging has attracted continued attention due to its beneficial characteristics of active release control (12,13), non-invasiveness (14,15), bio-orthogonality (4,7,16) and precision in temporal and spatial resolution (14,15). This is based on the concept of molecular caging (1,4,17) in which a molecule of interest is modified through its attachment with a photocleavable moiety ("cage") (3,18) such that its biological property is temporarily inactivated until its cage is detached by irradiation (4,17,19,20) (Fig. 1). Its development was pioneered by Hoffman. *et al*. (19) and Hess. *et al*. (20) as described in their influential works and has greatly expanded to a broad range of biological targets and functions (18) from cellular signaling (21–24), imaging (14), optogenetics (25–27), gene replication or regulation (16,25,28) to drug delivery systems (29–31).

Here, we have directed our interest of photocaging on acetylcholinesterase (AChE) due to its critical role in human physiology (32). AChE serves as a primary cholinesterase in the hydrolysis of acetylcholine, and it engages in the downregulation of excess acetylcholine released in neuronal synapses under normal physiological conditions (32). However, its loss of control can lead to an excessive downregulation of acetylcholine, serving a pathological basis implicated in the induction of neurodegenerative conditions and Alzheimer's disease (33). On the other hand, AChE is identified as a primary enzyme targeted and inactivated by reactive organophosphates (OPs) which are referred to as a class of neurotoxic chemicals that is comprised of nerve agents and agricultural pesticides such as paraoxon (POX) (34,35). Its inactivation by OPs occurs irreversibly via its covalent OP attachment as shown in its X-ray crystal structure (36) (Fig. 1b). This results in acetylcholine accumulation, and consequently, overstimulation at cholinergic synapses that constitutes a basis of acute OP neurotoxicity (34). However, this OP-inactivated AChE can be reactivated by treatment with an oxime class of antidote compounds which include 2-PAM and 4-PAM via nucleophilic catalysis (Fig. 1c) (37). Currently, caged oxime reactivators that target OP-inactivated AChE remain undeveloped despite their potential utility in AChE control. We believe that access to such compounds would be of significant value in their future applications potentially in the spatiotemporal control (14) of OP action (38), enzyme reactivation or antidote action.

In this current study, we are aiming on designing and validating caged oxime reactivators of AChE for their future use as molecular tools in the spatial and temporal control of AChE reactivation. Here, we wish to present our initial efforts on the design, synthesis and evaluations of caged oxime reactivators for their uncaging efficiency and biochemical activity *in vitro*. These efforts led to the identification of a novel caged reactivator and

*Corresponding author email: skchoi@umich.edu (Seok Ki Choi)
†This article is part of a Special Issue dedicated to the topic of Emerging Developments in Photocaging
© 2021 American Society for Photobiology

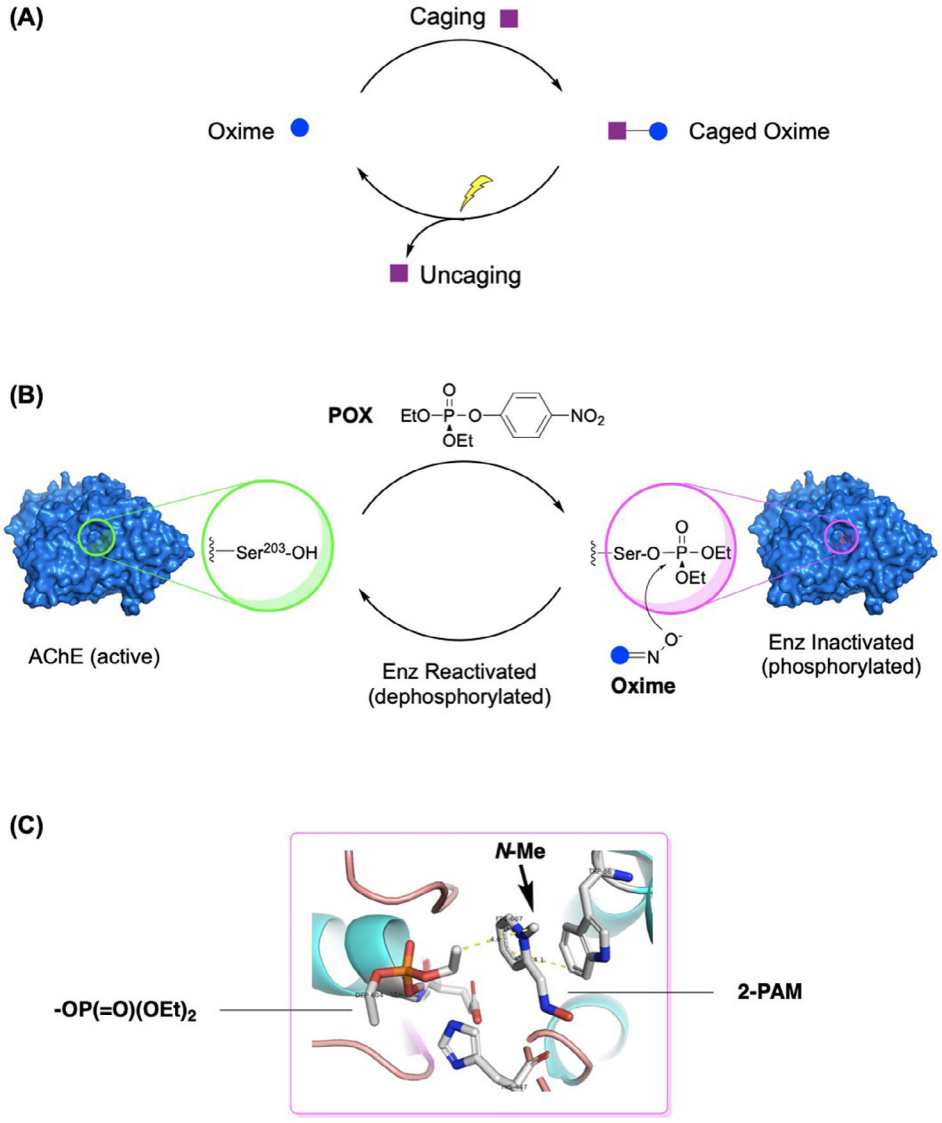

Figure 1. A photocaging strategy applied in the oxime reactivation of acetylcholinesterase (AChE). (a) A cartoon for oxime caging and uncaging controlled by light. (b) A schematic illustration of AChE for its irreversible inactivation by paraoxon (POX) at the catalytic site and its reactivation by an oxime reactivator through a mechanism of nucleophilic attack. (c) An X-ray crystal structure of POX-inactivated acetylcholinesterase (AChE-POX) complexed with 2-PAM (pdb 5HFA).

validation for its role in the control of AChE reactivation by light. To the best of knowledge, this study would represent a class of caged reactivators reported for the first time in the cholinesterase family of enzymes.

MATERIALS AND METHODS

Synthesis of caged oxime compounds. General: Chemicals used in the oxime synthesis are described in detail in the electronic Supporting Information along with analytical methods which include high-resolution mass spectrometry (HRMS), ^{1}H and ^{13}C NMR spectroscopy, and ultrahigh-performance liquid chromatography (UPLC).

Synthesis of N-(2-(dimethylamino)ethyl)-2-(hydroxyimino)acetamide (1, Scheme 1a): Oxime **1** was synthesized by reductive methylation of 2-(hydroxyimino)-*N*-(2′-aminoethyl)acetamide) **4** (39) as reported in literature (40). First, 2-(hydroxyimino)-*N*-(2′-aminoethyl)acetamide) (65 mg, 0.50 mmol) was added to excess formaldehyde in water (36.5–38%; 412 µL, 5.6 mmol), and the mixture was stirred for 30 min prior to the addition of sodium cyanoborohydride (176 mg, 2.8 mmol) as a solid. The mixture was heated at 50°C for 16 h and cooled to room temperature prior to its dilution with ether (5 mL), which led to white precipitates. This crude product was collected, washed with ether (2 × 5 mL) and further purified by flash column chromatography eluting with 10% methanol in dichloromethane. This afforded the desired product **1** as a white solid (52 mg, 65.9%). R_f (MeOH) = 0.1. Purity (UPLC): ≥95% (t_R = 1.98 min). HRMS (ESI-TOF) *m/z*: $[M–H]^-$ calcd for $C_6H_{13}N_3O_2^-$, 158.0930; found 158.0925. ^{1}H NMR (500 MHz, D_2O): δ 7.58 (s, 1H, CH = NOH), 3.59–3.57 (t, J = 5 Hz, 2H, CH_2NHC(=O)), 2.99–3.01 (t, J = 5 Hz, 2H, $CH_2N(CH_3)_2$), 2.62 (s, 6H, $N(CH_3)_2$) ppm. ^{13}C NMR (500 MHz, D_2O): δ 165.3, 143.6, 56.5, 43.3, 35.3 ppm.

Synthesis of N-((7-(diethylamino)-2-oxo-2H-chromen-4-yl)methyl)-2-(2-(hydroxyimino)acetamido)-N,N-dimethylethan-1-aminium bromide (2, Scheme 1b): First, compound **7**, an *N*-alkylation agent for coumarin caging, was prepared according to a literature protocol (41) as described in the Supporting Information. Then, a mixture of **1** (92 mg, 0.58 mmol) and 7-diethylaminocoumarin-4-methyl bromide **7** (90 mg, 0.29 mmol) dissolved in ethanol (3 mL) was heated at 45°C for 16 h. The reaction mixture was cooled to room temperature prior to dilution with ether

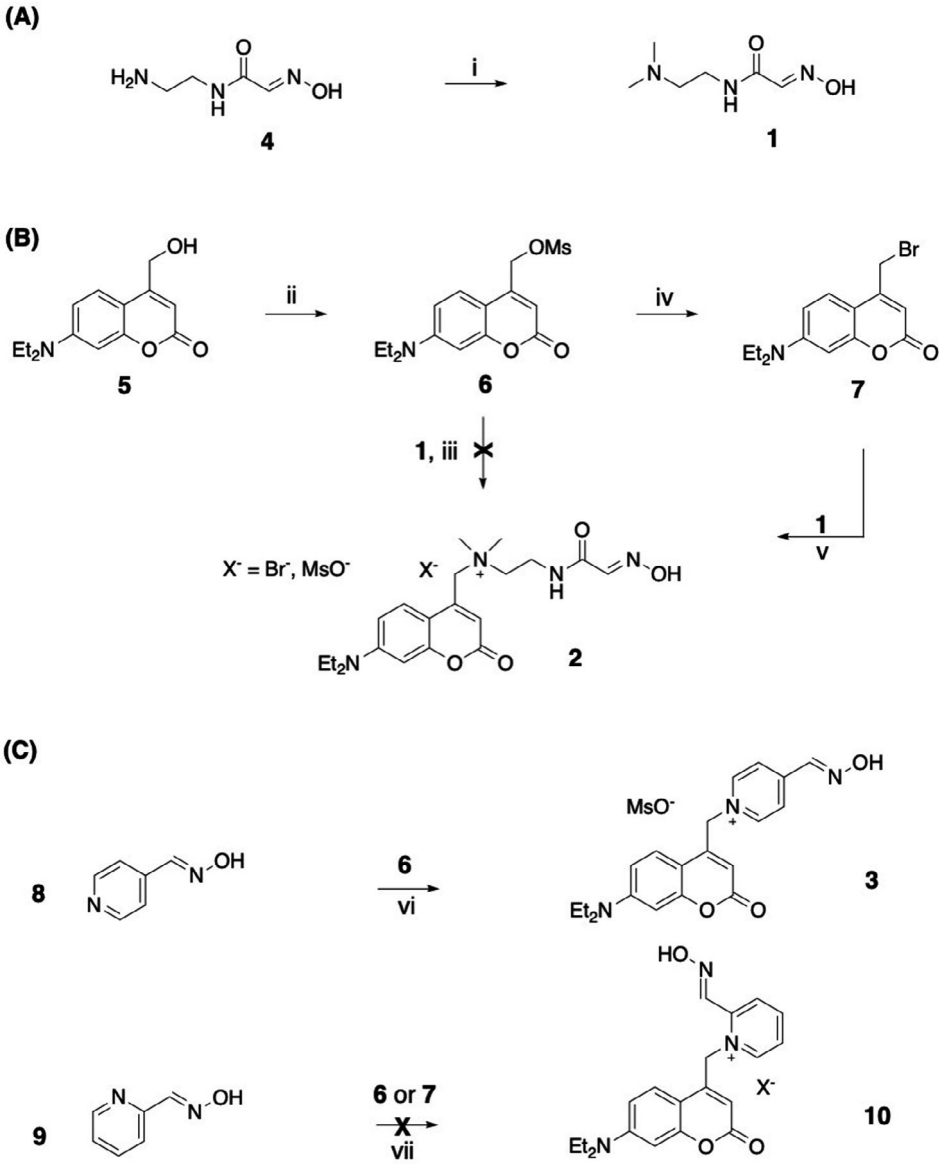

Scheme 1. Synthesis of caged oximes **2** and **3**. *Reagents and conditions*: (i) Formaldehyde, EtOH, 30 min, then $NaCNBH_3$, 50°C, 16 h (66%); (ii) Methanesulfonyl chloride (1.1 equiv), triethylamine (1.1 equiv), dichloromethane, rt, 1 h (73%); (iii) **1** (2.0 equiv), MeCN, 45°C, 24 h (decomposition); (iv) LiBr (3.0 equiv), THF, rt, 24 h (95%); (v) **1** (2.0 equiv), EtOH, 45°C, 16 h (70%); vi) **6** (1.0 equiv), **8** (2.5 equiv), MeCN, 45°C, 16 h (75%); (vii) **6** or **7** (1.0 equiv), **9** (2.5 equiv), MeCN, 45°C (no reaction) or 90°C, overnight (decomposition products). rt = room temperature..

(6 mL), which led to yellow precipitates. These were collected, washed with ether (3 × 3 mL) and further purified by crystallization in ethanol. The desired product **2** was obtained as a yellow solid (79 mg, 70%). Purity ≥95% (UPLC; Figure S5, Supporting Information. HRMS (ESI-TOF) *m/z*: $[M]^+$ calcd for $C_{20}H_{29}N_4O_4^+$, 389.2183; found 389.2369. ^{1}H NMR (500 MHz, D_2O): δ 7.68–7.66 (d, J = 10 Hz, 1H, H_5-DEACM), 7.60 (s, 1H, CH = NOH), 6.87–6.85 (d, J = 10 Hz, 1H, H_6-DEACM), 6.59 (s, 1H, H_8-DEACM), 6.30 (s, 1H, H_3-DEACM), 4.71 (s, 2H, 4-CH_2-DEACM), 3.93–3.90 (t, J = 8 Hz, 2H, $CH_2CH_2NHC(=O)$), 3.74–3.71 (t, J = 8 Hz, 2H, $CH_2CH_2NHC(=O)$), 3.48–3.44 (q, J = 7 Hz, 4H, 7-NEt_2-DEACM), 3.24 (s, 6H, $N^+(CH_3)_2$), 1.20–1.17 (t, J = 7 Hz, 6H, 7-NEt_2-DEACM) ppm. ^{13}C NMR (500 MHz, DMSO-d_6):162.6, 160.2, 156.4, 150.8, 143.41, 143.37, 141.9, 127.0, 115.5, 115.5, 108.9, 107.7, 97.3, 63.6, 61.4, 50.35, 4.14, 40.0, 33.1, 12.4 ppm.

Synthesis of 1-((7-diethylamino)-2-oxo-2H-chromen-4-yl)methyl)-4-((hydroxyimino)methyl)pyridin-1-ium methanesulfonate (3, Scheme 1c): A mixture of 7-diethylaminocoumarin-4-hydroxymethyl-*O*-methylsulfonate **6** (130 mg, 0.4 mmol) and 4-pyridinecarbaldehyde oxime **8** (122 mg, 1 mmol) dissolved in anhydrous acetonitrile (4 mL) was stirred at 45°C for 16 h and then refluxed at 90°C for an additional period of 40 min. Ether (20 mL) was added to the reaction mixture, which led to red precipitates. This solid material was collected, washed with ether (5 mL) and purified by flash silica column chromatography using 10% methanol in 1:1 acetone/dichloromethane as an eluant. This afforded the desired product **3** as a red solid (106 mg, 75%). R_f (20% methanol in 1:1 acetone/dichloromethane) = 0.2. Purity ≥95% (UPLC; Figure S5, Supporting Information). UV–vis spectroscopy (56 μM in phosphate buffered saline (PBS) pH 7.4): λ_{max} 397 nm (ε = 16,654 M^{-1} cm^{-1}), 270 nm (ε = 17,106 M^{-1} cm^{-1}). HRMS (ESI-TOF) *m/z*: $[M]^+$ calcd for $C_{20}H_{22}N_3O_3^+$, 352.1656; found 352.1755. ^{1}H NMR (500 MHz, CD_3OD): δ 9.00–8.98 (d, J = 10 Hz, 2H, pyridinium-*ortho*), 8.36 (s, 1H, CH = NHOH), 8.32–8.30 (d, J = 10 Hz, 2H, pyridinium-*meta*)), 7.53–7.51 (d, J = 10 Hz, 1H, H_5-DEACM), 6.80–6.77 (dd, J_1 = 5 Hz, J_2 = 10 Hz, 1H, H_6-DEACM), 6.61–6.60 (d, J = 5 Hz, 1H, H_8-DEACM), 6.04–6.03 (d, J = 5 Hz, 1H, H_3-DEACM), 5.51–5.50 (m, 2H, 4-CH_2-DEACM), 3.52–3.47 (q, J = 8 Hz, 4H, 7-NEt_2-DEACM), 2.69 (s, 3H, $CH_3SO_3^-$),

1.23–1.19 (t, $J = 7$ Hz, 6H, 7-NEt_2-DEACM) ppm. ^{13}C NMR (500 MHz, CD_3OD): 163.1, 157.6, 153.0, 152.4, 150.0, 146.9, 145.6, 126.0, 125.8, 110.7, 107.6, 106.7, 98.4, 60.7,45.7, 39.4, 29.5, 12.6 ppm.

Photolysis experiment. Light sources: Photolysis of caged oximes was performed by irradiation at either 365 nm under the lamp of long-wavelength ultraviolet (UVA) or 420 nm under the lamp of visible light, both available from Luzchem Research. Their photon flux density ($q_{n,p} = q_p/N_A$; mol s^{-1}) was determined as 1.90×10^{-7} (365 nm) and 1.30×10^{-7} (420 nm) by ferrioxalate actinometry as reported from our earlier work (42).

Photouncaging kinetics: In a representative experiment, a solution of caged oxime **2** or **3** (0.26 mM) dissolved in PBS pH 7.4 was placed at the distance of ~5 cm to a lamp and irradiated for 120 min. Its irradiated solution was periodically aliquoted as a function of irradiation time, and its aliquots were analyzed by UPLC and UV–vis spectrometry to determine the rate of oxime uncaging (Δoxime/Δt). High-performance liquid chromatography (HPLC)–mass spectrometry (ESI) was also employed for final aliquots to verify whether the released species was indeed identical to a molecular mass calculated for a free oxime (uncaged).

Quantum efficiency (Φ) in oxime uncaging was calculated as defined in Eq. 1 and Eq. 2 (43):

$$\Phi_{\text{uncaging}} = (\text{number of oxime uncaged})/(\text{number of photons absorbed}) \quad (1)$$

$$\Phi_{\text{uncaging}} = (\Delta\text{oxime}/\Delta t)/\left(q_{n,p}(1-10^{-A})\right) \quad (2)$$

where $q_{n,p}$ refers to photon flux density (mol s^{-1}), Δoxime/Δt refers to the rate of oxime uncaged (mol s^{-1}) and A refers to the absorbance of the coumarin cage molecule at the wavelength of irradiation.

AChE assay. Enzyme activity: This enzyme assay was performed *in vitro* using *Electrophorus electricus* AChE (0.2 U mL^{-1}) and acetylthiocholine (ATCh) as its substrate according to the Ellman's protocol in PBS pH 8.0 at 23°C (44,45). For enzyme kinetics, absorbance (A) at 412 nm was recorded as a function of time for up to 30 min as described in literature (39,40). These kinetic data were processed by plotting $A_{412\ nm}$ values against time (min). Enzyme activity was expressed in rate constant k (min^{-1}), which refers to the slope ($\Delta A_{412\ nm}/\Delta t$; min^{-1}) obtained at a linear phase of catalysis (0–15 min). Values of $k_{\text{POX or oxime}}$ refer to those determined in the plots of AChE treated with POX (caution: a hazardous material) or an oxime compound at a given concentration. These k values were used to calculate relative enzyme activity (%) as defined in Eq. 3:

$$\text{Enzyme activity}(\%) = 100 \times (k_{\text{POX or oxime}} - k_{\text{inactive}})/(k_{\text{active}} - k_{\text{inactive}}) \quad (3)$$

where k_{active} and k_{inactive} each refers to the rate constant of AChE either untreated (fully active) or treated with excess POX (AChE-POX; fully inactivated), respectively. Values of half-maximal inhibitory concentration (IC_{50}) were estimated from dose–activity response (%) curves through non-linear regression analysis.

Enzyme reactivation: In a 96-well microplate, AChE (0.2 U mL^{-1}; 0.18 mL in each well) was treated with POX (500 nM) for 30 min to reach its full inhibition at a residual activity of <5% and followed by the addition of 2-PAM or a test oxime in a designated range of concentrations (10^{-6}–10^{-3} M). After 30 min of additional incubation, the oxime-treated enzyme ("AChE-POX + Oxime") was assayed for its enzyme activity according to the protocol described above. The activity (%) of enzyme reactivation is defined in Eq. 4 (39,46):

$$\text{Reactivation activity}(\%) = 100 \times \left[\left(k_{(\text{POX}+\text{oxime})} - k_{\text{inactive}}\right)/(k_{\text{active}} - k_{\text{inactive}})\right] \quad (4)$$

where $k_{(\text{POX + oxime})}$ refers to the rate constant of AChE-POX treated with an oxime compound.

Light-controlled enzyme reactivation: In a 96-well microplate, AChE (0.2 U mL^{-1}, 0.18 mL in each well) was treated with both excess POX (500 nM) and a test oxime added at a variable range of concentrations (10^{-5}–10^{-3} M). Immediately, the microplate was placed under a lamp (365 nm, 420 nm) at the distance of ~5 cm and irradiated for 120 min. A duplicate plate was also prepared and left otherwise in the dark as a control. After photolysis, each solution in the well was assayed for enzyme activity by determining its k value as described above. The efficiency of enzyme reactivation is reported as % activity as defined in Eq. 5:

$$\text{Reactivation activity}(\%) = 100 \times \left[\left(k_{(\text{POX}+\text{oxime}+\text{hv})} - k_{\text{inactive}}\right)/(k_{\text{active}} - k_{\text{inactive}})\right] \quad (5)$$

where $k_{(\text{POX + oxime + hv})}$ refers to the rate constant determined for AChE-POX co-treated with an oxime under an irradiation condition.

RESULTS AND DISCUSSION

Design of caged oximes

Two types of oxime reactivators **2**, **3** were considered in the design of caged compounds for AChE reactivation as described in Fig. 2. Each of these contains a parent oxime reactivator that belongs in either a class of 2-(hydroxyimino)acetamide **1** (47,40) or *N*-methyl pyridinium-n-aldoxime (n-PAM) class of quaternary oximes such as 4-PAM (37). They have an identical coumarin moiety based on 6-diethylaminocoumarin-4-methyl (DEACM), a cage which is established for its rapid uncaging by irradiation of either a long-wavelength UV light (UVA) or visible light (27,42,48,49).

For its cage site, each parent oxime offers two distinct functionalities, each viable as the site of DEACM attachment as illustrated in **1** (Fig. 2a). This caging can occur at either its tertiary amine site (N-caging; arrow a) or the hydroxyl site of its oxime (O-caging; arrow b). We believed that either modification would result in its loss of binding affinity in the catalytic pocket and thus loss of original activity possibly due to steric interference induced upon putting the relatively bulky coumarin in the narrow valley of the *N*-Me or oxime-binding site (Fig. 1c) or due to its hydroxyl protection that abolishes the oxime nucleophilicity. However, in the current approach, we preferred the N-caging because of its easier synthesis which is achievable by one-step *N*-alkylation chemistry. This approach would yield an *N*-quaternary ammonium ion **2** or an *N*-quaternary pyridinium ion **3**, each as a caged form of **1** or 4-PAM, respectively. Another aspect considered against O-caging relates to potential occurrence of an N-O bond cleavage upon photolysis as postulated in Fig. 2b, which accounts for an undesired oxime fragmentation reported in *O*-benzoyl pyridinealdoximes (50). Instead, N-caging at the amine site allows desired uncaging via an N-C bond cleavage (51) as previously demonstrated with *N*-quaternary caged compounds of tertiary amines (52,53) and pyridines (54). In summary, we designed two types of caged compounds **2** and **3**, each tethered with DEACM at the site of tertiary amine or pyridine nitrogen.

Synthesis of caged oximes

Synthesis of **2** and **3** is described in Scheme 1. First, for the synthesis of **2**, its parent oxime **1** was prepared by the reductive *N*-methylation of its immediate precursor **4** (39) according to literature (40). Then, **1** was attempted for its *N*-quaternization reaction with **6**, an *O*-methanesulfonate-based alkylating molecule for DEACM (27). However, despite using excess oxime (2.0 equiv) under prolonged heating at 45°C, its reaction resulted in only an inseparable mixture of numerous spots in thin layer chromatography, indicative of reactant decompositions. This problem could be resolved by replacing **6** with **7**, a bromide analogue that offers a higher amine reactivity. Thus, its *N*-alkylation reaction with **7**, which was obtained by treating **6** with lithium bromide (41), afforded **2** with an isolation yield of 70%. This caged compound

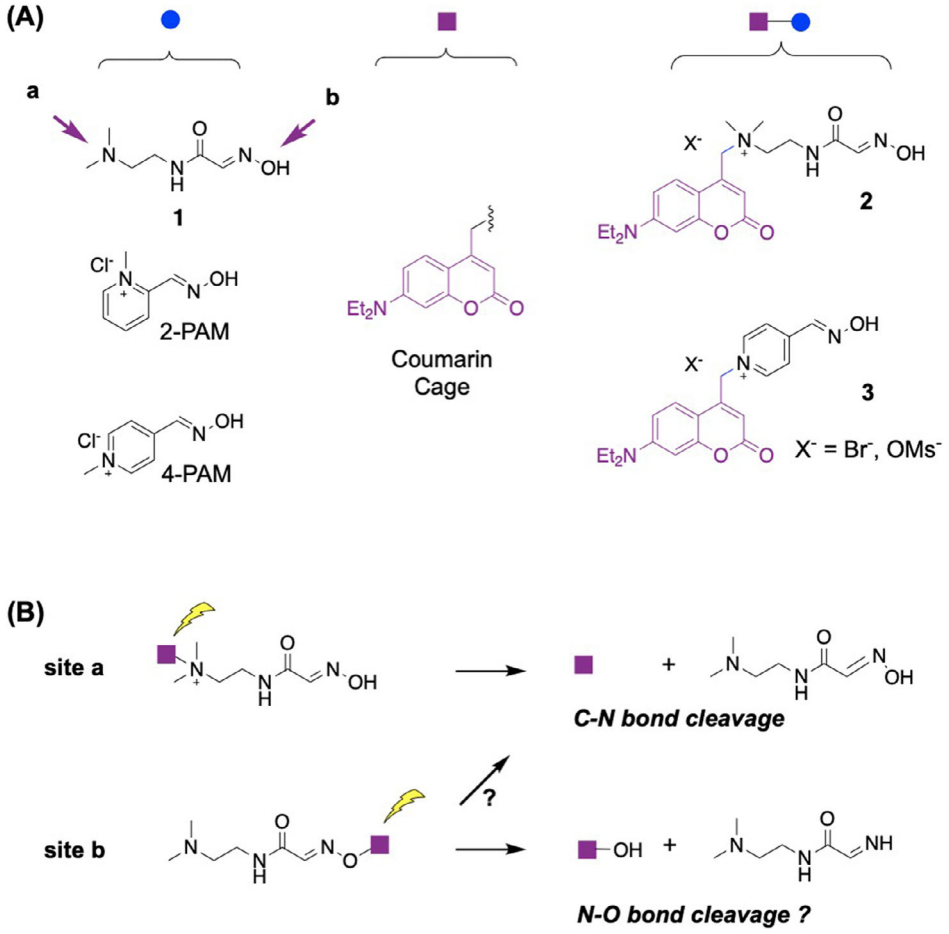

Figure 2. Design strategies of caged oxime reactivators. (a) Structures of oxime reactivators **1** and *N*-methyl pyridinium-n-aldoxime chloride (n-PAM; 2-PAM, 4-PAM). Two caged compounds **2** and **3** are designed, each attached with 7-diethylaminocoumarin-4-methyl (DEACM) at its amine nitrogen or pyridine nitrogen site, respectively. (b) Putative mechanisms of uncaging via photolytic cleavage at the C-N bond (N-caging, site a) or N-O bond (O-caging, site b).

was characterized for its purity ≥95% (UPLC; Figure S5, Supporting Information) and structural identity by standard analytical methods including HRMS (*m/z*): $[M]^+$ calcd for $C_{20}H_{29}N_4O_4^+$, 389.2183; found 389.2369 (Figure S2, Supporting Information).

Second, **3** was synthesized in a similar manner by the *N*-alkylation of **8** with **6** at its pyridine nitrogen. This caged compound was isolated in 75% yield with ≥95% purity (Figure S5, Supporting Information). Its identity was fully supported by various characterization data including UV–vis absorption peaks (397, 270 nm) and HRMS (*m/z*): $[M]^+$ calcd for $C_{20}H_{22}N_3O_3^+$, 352.1656; found 352.1755 (Figure S3, Supporting Information). We also attempted the synthesis of **10**, an ortho isomer to **3**, by applying the same alkylation condition to pyridine-2-aldoxime **9** (Scheme 1c). However, we were not able to achieve its successful *N*-quaternization reaction perhaps due to a severe steric repulsion generated by its aldoxime moiety located in close proximity to the pyridine nitrogen. In summary, two caged oximes **2** and **3** were prepared using an *N*-alkylation method.

Photouncaging kinetics of caged oximes

Caged oxime 2: Uncaging experiments were performed by irradiating with a long-wavelength UV light (UVA, 365 nm) or visible light (420 nm). These conditions have been frequently applied for DEACM uncaging due to its lack of cellular toxicity (27) and strong absorptivity (ε) by the coumarin chromophore in the targeted range of 340–440 nm (λ_{max} = 387 nm, ε = 22,687 M^{-1} cm^{-1}) (42,55). In a typical uncaging experiment, **2** (0.26 mM, PBS) was irradiated for up to 120 min, and its irradiated solution was monitored at various time points by UPLC analysis. Figure 3 shows two sets of overlaid UPLC traces, one acquired at irradiation at 365 nm and another at 420 nm. Each shows an exposure time-dependent decrease in **2** (t_r = 7.0 min) with the concomitant appearance of a new peak which was assigned as **1** (t_r = 1.6 min) along with another peak indicative of free coumarin **5** (t_r = 6.5 min) and a byproduct peak derived from coumarin (t_r = 7.6 min). This release kinetics is clearly supportive of desired uncaging via N-C bond cleavage in agreement with previously studies (52,53), but it offers no evidence for the occurrence of N-O bond cleavage as postulated in Fig. 2 b. Its uncaging kinetics were established as evident in the decay curves of **2** prepared by its area under curve (AUC) analysis in Fig. 3 (right). Comparison of its decay curves between the two light wavelengths confirms more rapid uncaging at 365 nm which led to an almost complete decay at 120 min compared with 420 nm which led to retention of **2** at a fraction of 0.29.

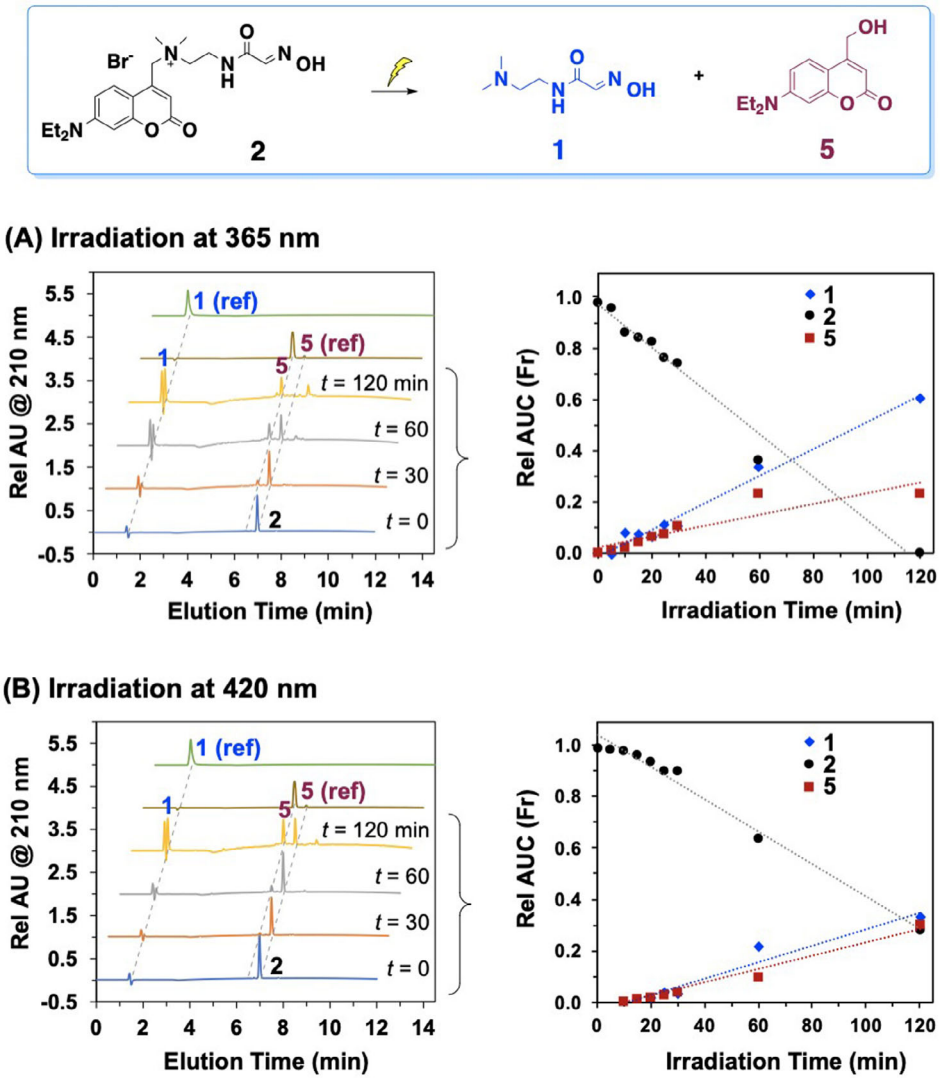

Figure 3. Photolysis of **2** performed under a long-wavelength UVA light (365 nm; a) or visible light (420 nm; b). (Left) Overlaid UPLC traces acquired at the detection channel of 210 nm. (Right) Fraction (Fr) in the area under curve (AUC) of each major peak plotted as a function of irradiation time. The photolysis was performed at 0.1 mg mL^{-1} (0.26 mM) in PBS pH 7.4 for an indicated period (0–120 min). The absorbance in each trace is presented in relative absorption unit (Rel AU).

The release of **1** detected in UPLC was further confirmed by its mass spectrometry analysis performed with a photolyzed solution at 120 min (Figure S6, Supporting Information). As anticipated, a mass spectral trace from the irradiation at 365 nm showed a predominant peak (*m/z*, found 160.1075), which is identical to **1** (*m/z*, calcd for $[M + H]^+ = 160.1086$). A similar mass analysis from 420 nm also confirmed the release of **1** in addition to residual **2** detected at a lower intensity. This data set is qualitatively in agreement with a conclusion drawn from UPLC traces in Fig. 3.

The uncaging efficiency of **2** was quantified by the regression analysis of each decay curve presented in Fig. 3. This analysis provided values for photochemical parameters which include rate of uncaging ($k_{uncaging}$, mol s^{-1}), quantum efficiency (Φ) and sensitivity ($\Phi \times \varepsilon$) as summarized in Table 1. Their values confirmed dependence of uncaging on irradiation wavelength as evident with the greater decay rate and higher sensitivity of uncaging at 365 nm compared with 420 nm. Moreover, the results indicated slower uncaging kinetics of **2** compared with other coumarin-caged compounds reported from our laboratories including tamoxifen (42) and thymidine (27), each DEACM caged at their phenolic site. This may partly reflect differences in leaving group property, suggesting slower release by a tertiary amine compared with a phenol.

Caged oxime 3: Compound **3**, which is caged at the pyridine nitrogen site, was investigated for its uncaging kinetics by irradiation at 365 nm. Contrary to our anticipation, it remained stable even after 120 min of irradiation as indicated by UPLC traces presented in Fig. 4. Its structural basis that contributed to such photostability remains undetermined, though our literature review later suggests its cage attachment at the pyridine nitrogen as the basis because even an unsubstituted pyridine caged at the nitrogen atom with DEACM also displayed a very low level of uncaging sensitivity ($\Phi_{405\ nm} \times \varepsilon = 0.28$) (54). That study attributed its poor uncaging property to the occurrence of photoinduced intramolecular electron transfer (56) at the pyridinium ring as a

Table 1. Photochemical properties of caged oxime **2** and released products[a]

	2	1		5	
Irradiation Wavelength	$k_{uncaging} \times 10^9$	$\Phi \times 10^3$	$\Phi \bullet \varepsilon$	$\Phi \times 10^3$	$\Phi \bullet \varepsilon$
365 nm	2.2 (±0.57)	6.0 (±0.3)	94.4 (±5.3)	5.3 (±1.3)	83.4 (±20.8)
420 nm	1.4 (±0.15)	5.4	41.9 (±0.2)	4.8 (±0.8)	37.1 (±6.6)

[a] Each value represents a mean ± standard deviation (SD) associated with two decay or production curves acquired at the detection wavelengths of 210 and 285 nm. $k_{uncaging}$ = rate of uncaging (mol s^{-1}). Φ = quantum efficiency of release. Φ•ε = sensitivity of uncaging at the wavelength (λ) of irradiation (M^{-1} cm^{-1}).

potential mechanism that overrides the desired route of C-N bond cleavage. Due to this uncaging deficiency, **3** was not further considered in the light-controlled experiments of AChE catalysis as described below.

Evaluation of Oxime Activity in AChE Catalysis

Prior to reactivation experiments, **1** and **2** were studied for their potential activities in intact AChE as postulated in Fig. 5. This assay was performed *in vitro* using AChE from *Electrophorus electricus* and ATCh as its substrate according to the Ellman's protocol (44). First, POX was validated as a positive control for enzyme inactivation (39,40) as presented in the kinetic traces of ATCh hydrolysis in Fig. 6a. Indeed, treatment of AChE with POX resulted in a dose-dependent decrease in its catalytic rate ($k = \Delta A_{412\ nm}/\Delta t$; min^{-1}) or equivalently enzyme activity (%) as each plotted in Figure S7A (Supporting Information) and Fig. 6 d, respectively. This confirmed strong inactivation by POX with a half-maximal inhibitory concentration (IC_{50}) of 15 nM, which is in close agreement with literature values (39,40).

Evaluation of **1** and **2** was performed under an identical assay condition otherwise at a higher range of concentrations (1.0 μ M–1.0 mM). Kinetic traces obtained from the enzyme treated with **1** apparently show only minor variations (Fig. 6b) though their regression analysis for enzyme activity suggested a stimulatory effect with an increase to120–130% at 0.1–1.0 mM (Fig. 6e). This increase is believed to be rather insignificant or only modest considering the standard deviation of error (±7%) by untreated AChE. Additionally, this might be attributable to the non-enzymatic hydrolysis of ATCh by oxime, which is known to occur at millimolar concentrations (39). Interestingly, the caged compound **2** showed enzyme inhibition in a dose-dependent manner as shown in Fig. 6c, d. Its IC_{50} value of 21 μM indicates an inhibitory activity, which is approximately three orders of magnitude less potent than POX. Despite its weaker activity, **2** illustrates a gain-of-function after caging, which is absent in its parent oxime **1**.

Reactivation of POX-inactivated AChE (AChE-POX)

Free oxime **1** was tested for verifying its activity in AChE reactivation without light irradiation. In this assay, AChE was fully inactivated by treatment with excess POX at 500 nM (>>IC_{50}) for 30 min prior to the incubation of the resulting AChE-POX

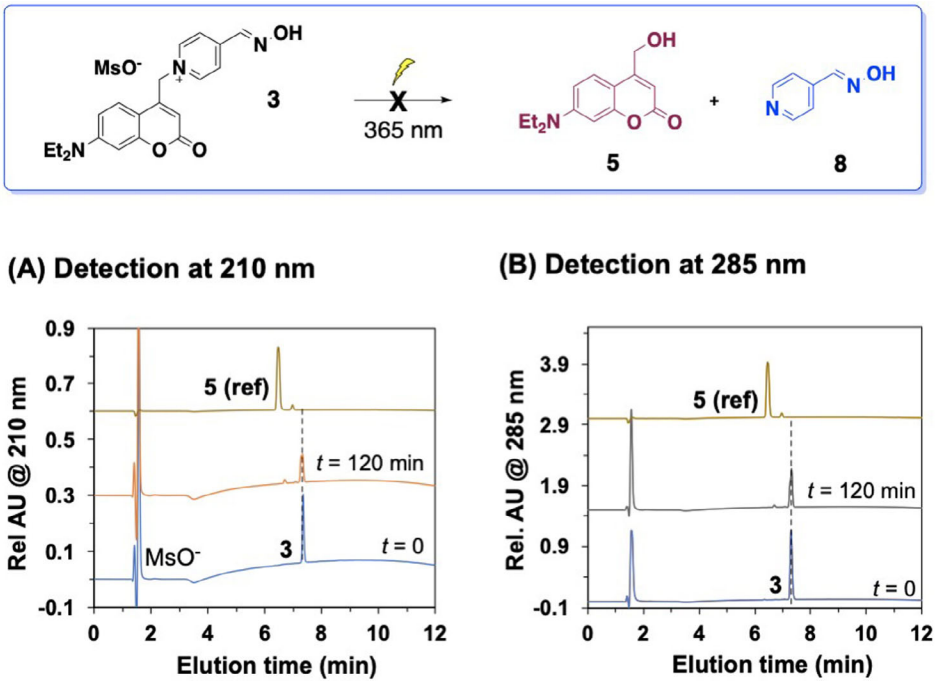

Figure 4. Photolysis of **3** performed at long-wavelength UVA (365 nm). Representative UPLC traces acquired at the detection channel of 210 nm (a) or 285 nm (b). The photolysis was performed at 0.1 mg mL^{-1} (0.28 mM) in PBS pH 7.4 for 120 min.

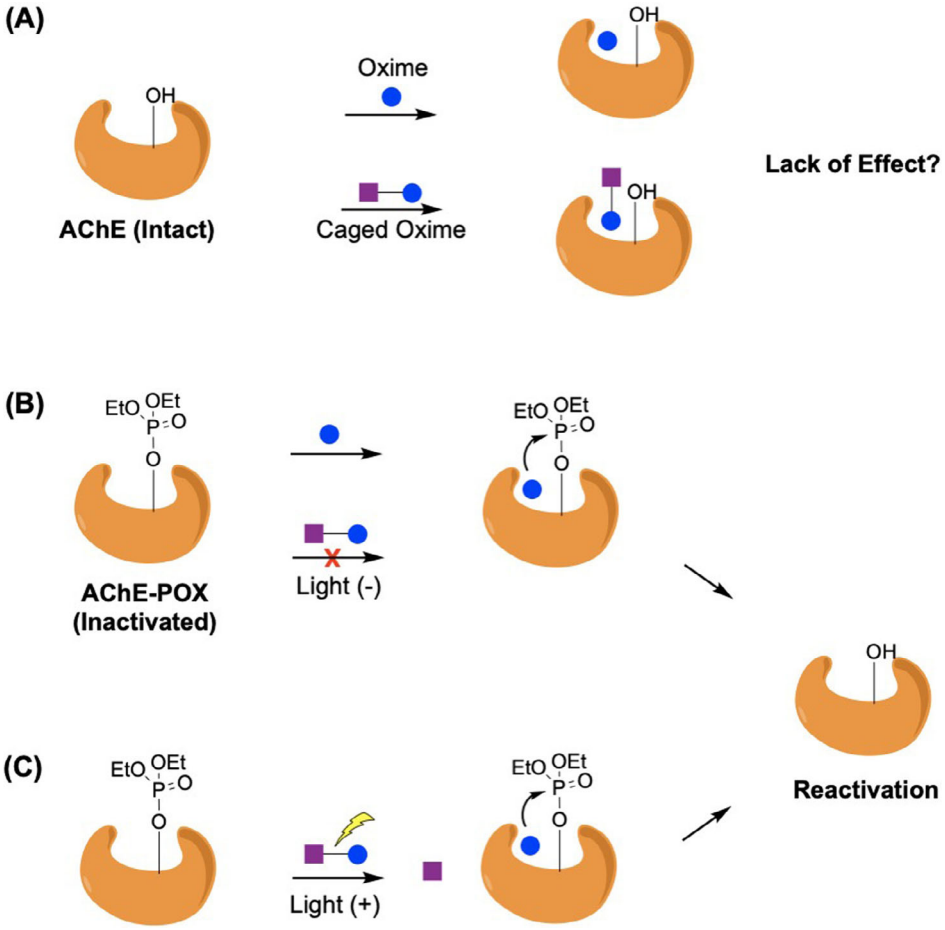

Figure 5. Putative modes of action in AChE by an oxime reactivator and its caged molecule. (a) Effects on the native enzyme where its catalytic function can be potentially affected due to co-occupation by the caged moiety. (b, c) Reactivation of POX-inactivated enzyme where its original function can be restored by either free oxime or caged oxime via photolytic uncaging.

with **1** or 2-PAM as a standard reactivator (10^{-6}–10^{-3} M). Each of these compounds displayed ability for enzyme reactivation as evident in the kinetic traces of enzyme catalysis (Fig. 7a, b) and quantified in the plots of enzyme activity (Fig. 7d).

2-PAM (46,57) showed a growth of activity plateaued (75%) at 10 μM after which it gradually decreased at higher concentrations. Its biphasic trend in the dose–activity curve has been already noted in a few reports (39,58), which is attributed to the competitive inhibition of enzyme by 2-PAM around millimolar concentrations. Compound **1** showed reactivation activity though less active than 2-PAM at 0.1 mM or lower concentrations. However, unlike 2-PAM, **1** showed a dose-dependent growth of activity in its entire range of test concentrations, which resulted in a greater activity (115%) at 1 mM compared with ~40% by 2-PAM.

Finally, despite its lack of uncaging property (Fig. 4), **3** was also included in this assay for evaluating the functional consequence of its cage attachment. Its assay performed in a comparable range of concentrations (1.0–100 μM) to 2-PAM showed a significant but incomplete loss of activity (Fig. 7c, d). Thus, it retained an activity of up to 24% which is approximately 3-fold less compared with 2-PAM. This suggests that cage attachment at the pyridinium nitrogen site appears effective but not enough for fully masking the original activity before caging.

In summary, we evaluated **1** and two comparators with regards to their activities in the reactivation of POX-inactivated AChE *in vitro*. Compound **1** was weaker than 2-PAM at micromolar concentrations but comparable with or better at millimolar concentrations.

Light-controlled reactivation of AChE-POX

The enzyme assay was then focused on the control of enzyme reactivation under variable light conditions (Fig. 8). We performed control experiments first to ensure that light irradiation alone would make no impact on the action of AChE, POX or free oxime **1**. These involved the irradiation of AChE treated with either POX (500 nM) or POX + **1** (0.3 mM) to either a UVA light (365 nm) or blue light (420 nm) for 120 min (Fig. 8 a). The kinetic traces of the enzyme treated with POX alone ("AChE-POX" ± Light) indicate occurrence of full inactivation under all conditions regardless of irradiation or light wavelength. On the other hand, the kinetic traces of AChE alone (not shown) or the enzyme treated with both POX and **1** ("AChE-POX + **1**" ± Light) show retention of effective enzyme catalysis apparently with little variation under all three conditions. Indeed, their values in rate constant (Fig. 8c) or equivalently enzyme activity (%) (Fig. 8d) extracted from their traces confirm only a

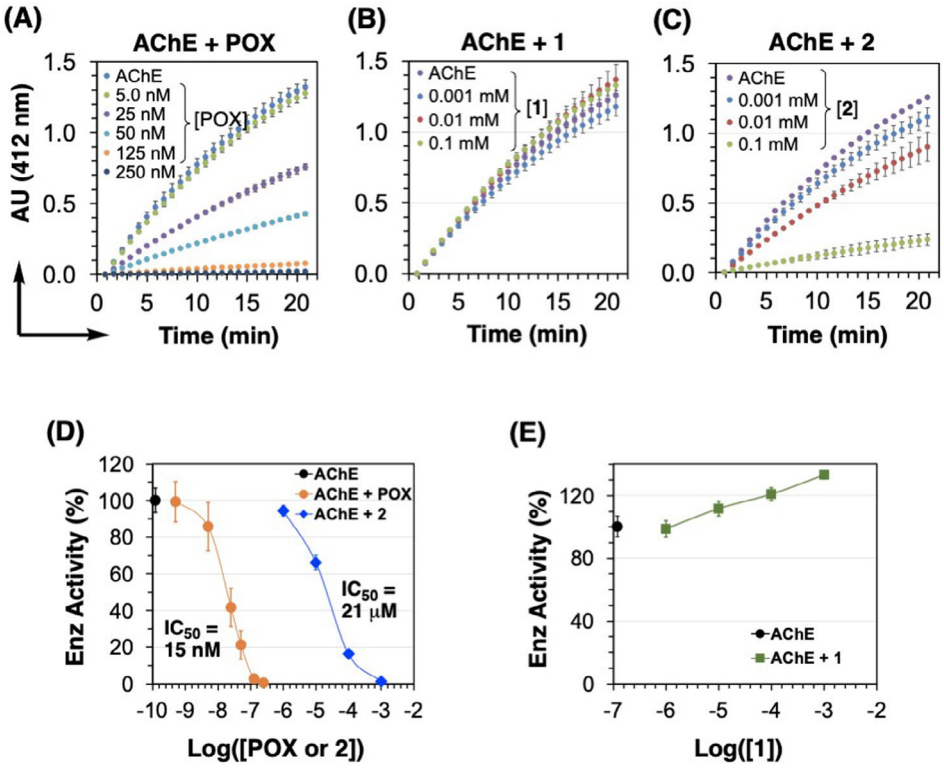

Figure 6. Activities of paraoxon (POX), **1** and **2** on the catalytic activity of AChE *in vitro*. (a–c) Kinetic traces of acetylthiocholine hydrolysis by *Electrophorus electricus* AChE (0.2 U mL^{-1}), and (d, e) Plots of dose-dependent enzyme activity (%). Each data point refers to a mean ± standard deviation (SD, $n = 3$).

small range of variations from 58% (no light), 51% (365 nm) to 49% (420 nm). Overall, these control experiments corroborate a lack of noticeable impact by irradiation on enzyme catalysis, its inactivation by POX or reactivation by **1**.

We proceeded to light-controlled enzyme reactivation using **2** at 0.3 mM where its parent oxime **1** showed a reactivation activity of 58% (Fig. 7d). Here, AChE treated with POX and **2** (AChE-POX + **2**) was either left in the dark or irradiated for 120 min prior to measurement of its reactivation activity. The treated enzyme without irradiation showed only a stochastic variation in enzyme kinetics (left, Fig. 8b; Figure S9, Supporting Information), an evidence indicative of a lack of enzyme reactivation in addition to enzyme inhibition by intact **2** (Fig. 6d). This is contrasted with two light-exposed traces, each acquired after irradiation at either 365 nm (middle) or 420 nm (right) that shows solidly a linear growth in catalysis. We believe that each of these two curves is clearly supportive of the occurrence of enzyme reactivation as the result of light-controlled oxime release.

The extent of enzyme reactivation induced by irradiation was quantified in rate constant (k, min^{-1}) as presented in Fig. 8c. The rate constant under no light condition could not be determined due to stochastic kinetic traces (Figure S9, Supporting Information), suggesting lack of enzyme activity occurred. Otherwise, its k values include 4.3×10^{-3} at 365 nm and 3.4×10^{-3} at 420 nm (yellow bars), each of which indicates approximately 10-fold faster catalysis than the k value ($3.3–4.4 \times 10^{-4}$) obtained from the AChE-POX irradiated without **2** (orange bars). These two values are equivalent to 6.5 ± 0.7% and 5.4 ± 1.3% in enzyme activity, respectively, as plotted in Fig. 8d. This level of activity is 9- to 10-fold lower compared with the reactivation activity (58%) offered by free oxime **1** at an identical dose (0.3 mM; Fig. 7 d). Such reduction might be attributable to a few factors that relate to suboptimal yields of uncaging and importantly the inhibitory activity conferred by remaining **2** (Fig. 6d). On the other hand, we believe that effects by coumarin **5** and its byproduct might be insignificant as evident with a lack of reactivation activity by **5** (0.9 ± 0.5% at 0.1 mM; not shown).

In summary, **2** was evaluated in a series of AChE reactivation experiments controlled under variable light conditions. This caged compound lacked an activity for enzyme reactivation in the dark. However, after irradiation, it was able to restore some of its pre-caging activity, proving its important role in the temporal control of AChE reactivation by light.

CONCLUSION

In this study, we designed two coumarin-caged compounds **2** and **3** each as a photoactivatable reactivator for AChE. We evaluated their uncaging kinetics in solution and measured their biochemical activities in AChE assays *in vitro*. This study provided evidence supportive of the light-dependent control of AChE reactivation by **1**. This result is of significance because it describes a first class of caged compounds validated in the light control of AChE catalysis. It also offers novel insights into their design and addresses challenges that face the advances in photocaging application.

First, we find it challenging to predict a desired functional outcome via caging in the oxime class of AChE reactivators.

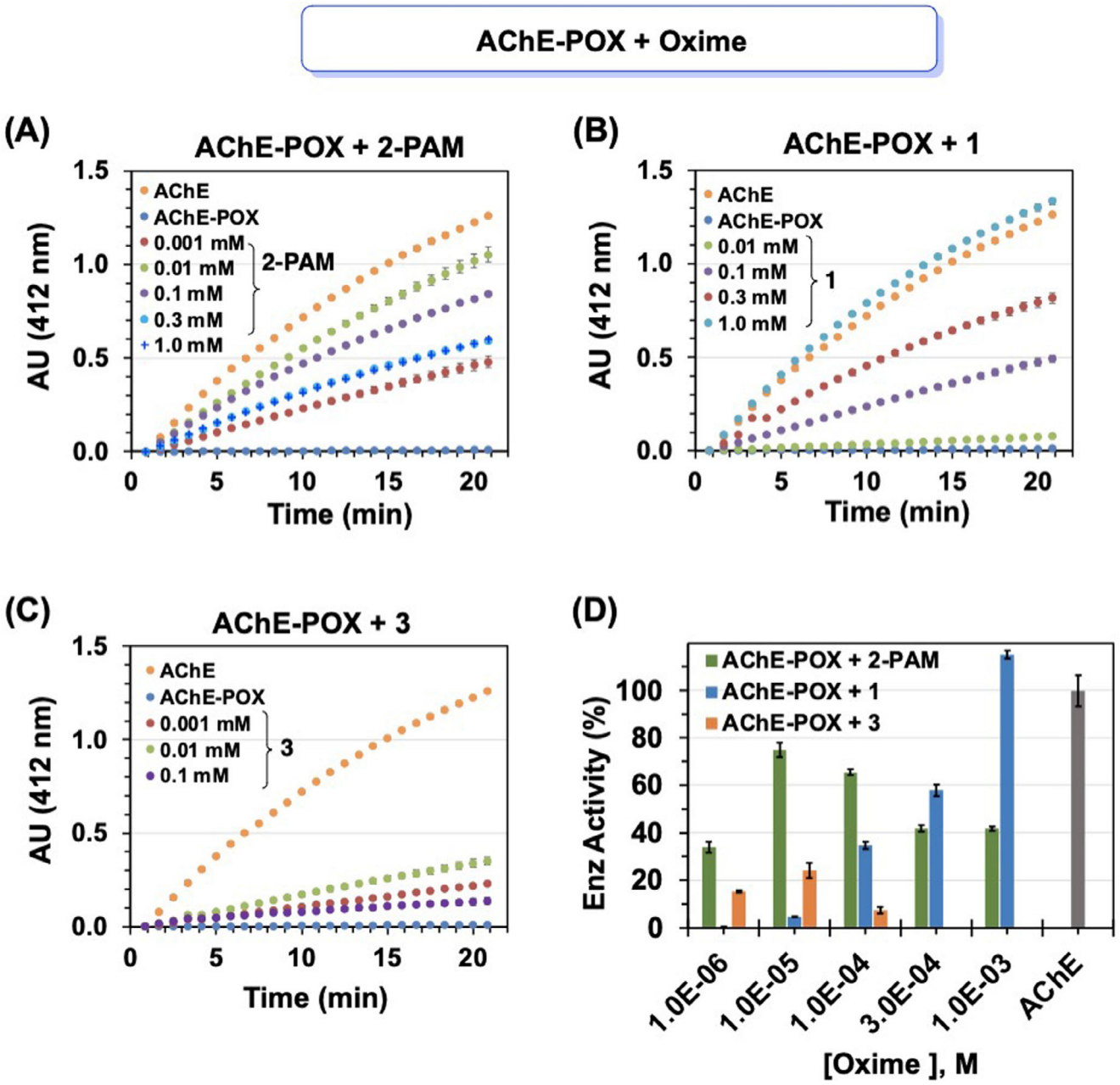

Figure 7. Reactivation of POX-inhibited AChE by oximes *in vitro*. (a–c) Kinetic traces of acetylthiocholine hydrolysis by AChE-POX (500 nM) that show dose-dependent reactivation by 2-PAM, **1** and **3**. (d) Plots of enzyme activity (%) against oxime concentration. Each data point refers to a mean ± SD ($n = 3$).

This is illustrated with an inhibitory activity of **2** observed in AChE catalysis, which was absent in its parent oxime **1**. Although much weaker and reversible compared with inhibition by POX, this new activity could interfere with AChE catalysis unless **2** becomes completely uncaged after photolysis. Additionally, **3** retained some level of activity in AChE reactivation, which is less desirable than its complete loss of activity.

Second, the photostability displayed by **3** made it inapplicable for light-controlled enzyme reactivation. This problem did not occur in the quaternary ammonium ion **2**, suggesting a potential role by its pyridinium ion. This might be linkable in part to the mechanism of electron transfer at the pyridinium ring as suggested in earlier studies (54,56). This issue is likely addressable in the future by using other cage types or more effective cages made of an ortho-nitrobenzyl (13,59), 8-cyano-7-hydroxyquinolinyl (52) and 3-iodo-7-diethylaminocoumarin core (54) in combination with irradiation at longer wavelengths which is known to suppress the rate of undesired photoelectron transfer (60).

In conclusion, this study developed a photocaging application for AChE catalysis which was demonstrated in the context of light-dependent control of enzyme reactivation *in vitro*. It identified challenges and areas for improvement such as in the cage design for oxime reactivators. Their potential to serve in the spatiotemporal control of AChE reactivation remains a subject for future efforts.

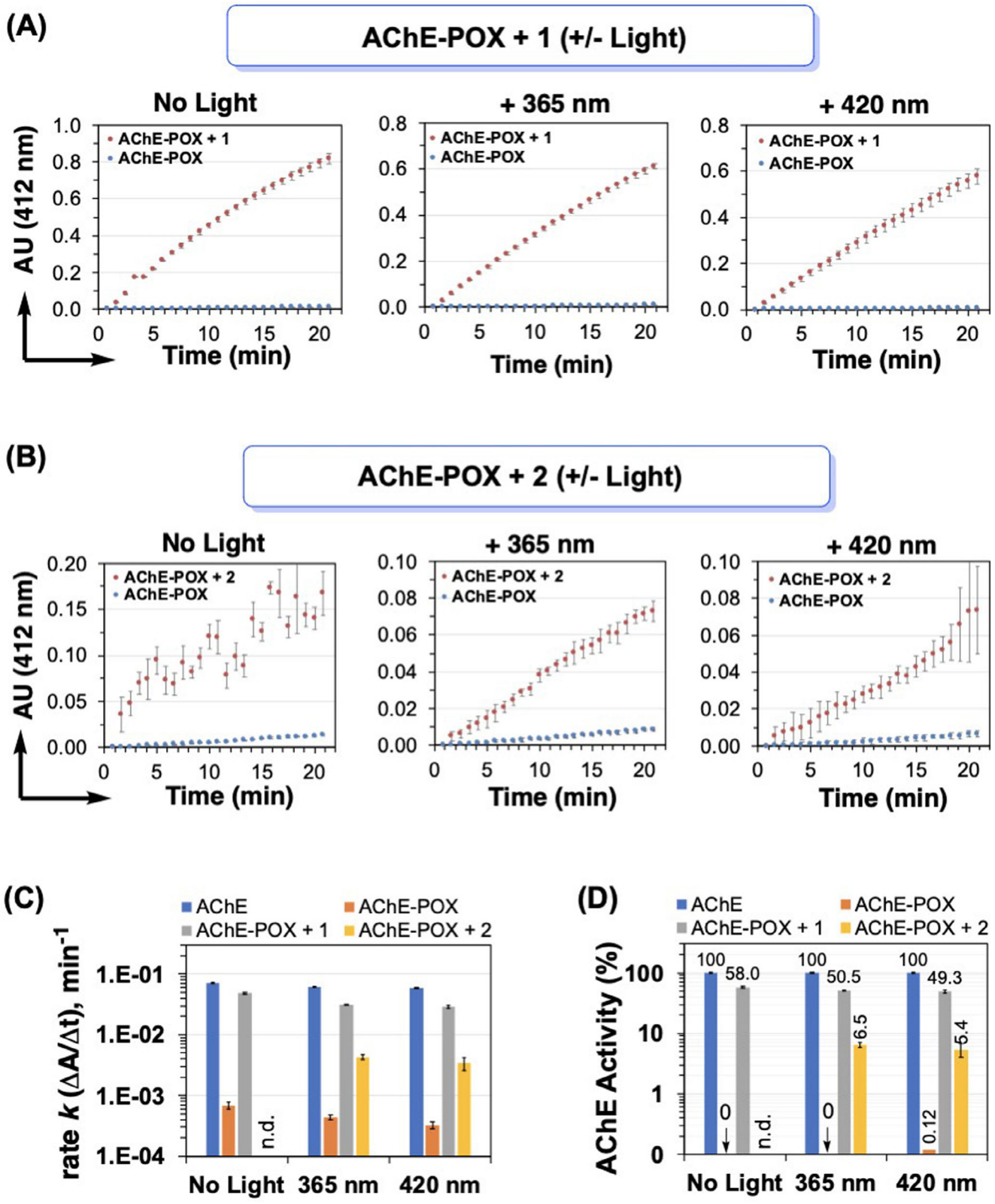

Figure 8. Light-controlled reactivation of POX-inhibited AChE by oximes **1**, **2** *in vitro*. (a, b) Kinetic traces of acetylthiocholine hydrolysis by AChE-POX (500 nM) after treatment with **1** or **2**, each at 0.3 mM, under variable conditions (± light, 2 h). (c, d) Plots of rate constant values (k, min^{-1}) and corresponding enzyme activities (%) against treatment conditions. Each data point refers to a mean ± SD (n = 3). n.d. = not determined.

Acknowledgements—This work was supported by the US Defense Threats Reduction Agency–DOD [HDTRA1-17-C-00001].

SUPPORTING INFORMATION

Additional supporting information may be found online in the Supporting Information section at the end of the article:

S1. Materials and Analytical Methods

S2. Synthetic Methods of **4**–**7**

Figure S1. Copies of spectra (mass, ^{1}H & ^{13}C NMR) of oximes **1**.

Figure S2. Copies of spectra (mass, ^{1}H & ^{13}C NMR) of oximes **2**.

Figure S3. Copies of spectra (mass, ^{1}H & ^{13}C NMR) of oximes **3**.

Figure S4. Copies of spectra (mass, ^{1}H & ^{13}C NMR) of oximes **7**.

Figure S5. UPLC traces of **1**–**3**, **5**

Figure S6. HPLC-mass spectrometry analysis of **2** after photolysis.

Figure S7. Plots of k values of AChE after treatment with POX, **1**, **2**.

Figure S8. Plots of k values of AChE-POX after oxime treatment.

Figure S9. Kinetic traces of acetylthiocholine hydrolysis under dark conditions.

REFERENCES

1. Ellis-Davies, G. C. R. (2020) Useful caged compounds for cell physiology. *Acc. Chem. Res.* **53**, 1593–1604.
2. Lou, J. and M. D. Best (2020) Reactive oxygen species-responsive liposomes via boronate-caged phosphatidylethanolamine. *Bioconjugate Chem* **31**, 2220–2230.
3. Yu, H., J. Li, D. Wu, Z. Qiu and Y. Zhang (2010) Chemistry and biological applications of photo-labile organic molecules. *Chem. Soc. Rev.* **39**, 464–473.
4. Brieke, C., F. Rohrbach, A. Gottschalk, G. Mayer and A. Heckel (2012) Light-controlled tools. *Angew. Chem. Int. Ed.* **51**, 8446–8476.
5. Lerch, M. M., M. J. Hansen, G. M. van Dam, W. Szymanski and B. L. Feringa (2016) Emerging targets in photopharmacology. *Angew. Chem. Int. Ed.* **55**, 10978–10999.
6. Dcona, M. M., K. Mitra and M. C. T. Hartman (2020) Photocontrolled activation of small molecule cancer therapeutics. *RSC Med. Chem.* **11**, 982–1002.
7. Velema, W. A., J. P. van der Berg, W. Szymanski, A. J. M. Driessen and B. L. Feringa (2014) Orthogonal control of antibacterial activity with light. *ACS Chem. Biol.* **9**, 1969–1974.
8. Wang, Y. and D. S. Kohane (2017) External triggering and triggered targeting strategies for drug delivery. *Nat. Rev. Mater.* **2**, 17020.
9. Choi, S. K. (2020) Photoactivation Strategies for Therapeutic Release in Nanodelivery Systems. *Adv. Ther. (Weinheim, Ger.)* **3**, 2000117.
10. Alvarez-Lorenzo, C., L. Bromberg and A. Concheiro (2009) Light-sensitive Intelligent Drug Delivery Systems. *Photochem. Photobiol.* **85**, 848–860.
11. Zhu, J., T. Xiao, J. Zhang, H. Che, Y. Shi, X. Shi and J. C. M. van Hest (2020) Surface-charge-switchable nanoclusters for magnetic resonance imaging-guided and glutathione depletion-enhanced photodynamic therapy. *ACS Nano* **14**, 11225–11237.
12. Nani, R. R., A. P. Gorka, T. Nagaya, H. Kobayashi and M. J. Schnermann (2015) Near-IR light-mediated cleavage of antibody-drug conjugates using cyanine photocages. *Angew. Chem. Int. Ed.* **54**, 13635–13638.
13. Mahmoodi, M. M., D. Abate-Pella, T. J. Pundsack, C. C. Palsuledesai, P. C. Goff, D. A. Blank and M. D. Distefano (2016) Nitrodibenzofuran: A one- and two-photon sensitive protecting group that is superior to brominated hydroxycoumarin for thiol caging in peptides. *J. Am. Chem. Soc* **138**, 5848–5859.
14. Furuta, T., S. S. H. Wang, J. L. Dantzker, T. M. Dore, W. J. Bybee, E. M. Callaway, W. Denk and R. Y. Tsien (1999) Brominated 7-hydroxycoumarin-4-ylmethyls: Photolabile protecting groups with biologically useful cross-sections for two photon photolysis. *Proc. Natl. Acad. Sci. U. S. A.* **96**, 1193–1200.
15. Nani, R. R., A. P. Gorka, T. Nagaya, T. Yamamoto, J. Ivanic, H. Kobayashi and M. J. Schnermann (2017) In Vivo activation of duocarmycin-antibody conjugates by near-infrared light. *ACS Cent. Sci.* **3**, 329–337.
16. Fichte, M. A. H., X. M. M. Weyel, S. Junek, F. Schäfer, C. Herbivo, M. Goeldner, A. Specht, J. Wachtveitl and A. Heckel (2016) Three-dimensional control of DNA hybridization by orthogonal two-color two-photon uncaging. *Angew. Chem. Int. Ed.* **55**, 8948–8952.
17. Lee, H.-M., D. R. Larson and D. S. Lawrence (2009) Illuminating the chemistry of life: design, synthesis, and applications of "caged" and related photoresponsive compounds. *ACS Chem. Biol.* **4**, 409–427.
18. Klán, P., T. Šolomek, C. G. Bochet, A. Blanc, R. Givens, M. Rubina, V. Popik, A. Kostikov and J. Wirz. (2013) Photoremovable protecting groups in chemistry and biology: Reaction mechanisms and efficacy. *Chem. Rev.* **113**, 119–191.
19. Kaplan, J. H., B. Forbush and J. F. Hoffman (1978) Rapid photolytic release of adenosine 5'-triphosphate from a protected analog: Utilization by the sodium: Potassium pump of human red blood cell ghosts. *Biochemistry* **17**, 1929–1935.
20. Billington, A. P., K. M. Walstrom, D. Ramesh, A. P. Guzikowski, B. K. Carpenter and G. P. Hess (1992) Synthesis and photochemistry of photolabile N-glycine derivatives and effects of one on the glycine receptor. *Biochemistry* **31**, 5500–5507.
21. Amatrudo, J. M., J. P. Olson, G. Lur, C. Q. Chiu, M. J. Higley and G. C. R. Ellis-Davies (2014) Wavelength-selective one- and two-photon uncaging of GABA. *ACS Chem. Neurosci.* **5**, 64–70.
22. Kantevari, S., M. Matsuzaki, Y. Kanemoto, H. Kasai and G. C. R. Ellis-Davies (2010) Two-color, two-photon uncaging of glutamate and GABA. *Nat. Methods* **7**, 123–125.
23. Karginov, A. V., Y. Zou, D. Shirvanyants, P. Kota, N. V. Dokholyan, D. D. Young, K. M. Hahn and A. Deiters (2011) Light regulation of protein dimerization and kinase activity in living cells using photocaged rapamycin and engineered FKBP. *J. Am. Chem. Soc.* **133**, 420–423.
24. Lemke, E. A., D. Summerer, B. H. Geierstanger, S. M. Brittain and P. G. Schultz (2007) Control of protein phosphorylation with a genetically encoded photocaged amino acid. *Nat. Chem. Biol.* **3**, 769–772.
25. Link, K. H., Y. Shi and J. T. Koh (2005) Light activated recombination. *J. Am. Chem. Soc.* **127**, 13088–13089.
26. Lu, X., S. S. Agasti, C. Vinegoni, P. Waterman, R. A. DePinho and R. Weissleder (2012) Optochemogenetics (OCG) allows more precise control of genetic engineering in mice with CreER regulators. *Bioconjugate Chem.* **23**, 1945–1951.
27. Wong, P. T., E. W. Roberts, S. Tang, J. Mukherjee, J. Cannon, A. J. Nip, K. Corbin, M. F. Krummel and S. K. Choi (2017) Control of an unusual photo-claisen rearrangement in coumarin caged tamoxifen through an extended spacer. *ACS Chem. Biol.* **12**, 1001–1010.
28. Zhou, W., W. Brown, A. Bardhan, M. Delaney, A. S. Ilk, R. R. Rauen, S. I. Kahn, M. Tsang and A. Deiters (2020) Spatiotemporal control of CRISPR/Cas9 function in cells and zebrafish using light-activated guide RNA. *Angew. Chem. Int. Ed.* **59**, 8998–9003.
29. Agasti, S. S., A. M. Laughney, R. H. Kohler and R. Weissleder (2013) A photoactivatable drug-caged fluorophore conjugate allows direct quantification of intracellular drug transport. *Chem. Commun.* **49**, 11050–11052.
30. Dupart, P. S., K. Mitra, C. E. Lyons and M. C. T. Hartman (2019) Photo-controlled delivery of a potent analogue of doxorubicin. *Chem. Commun.* **55**, 5607–5610.
31. Wong, P., S. Tang, J. Mukherjee, K. Tang, K. Gam, D. Isham, C. Murat, R. Sun, J. R. Baker and S. K. Choi (2016) Light-controlled active release of photocaged ciprofloxacin for lipopolysaccharide-

targeted drug delivery using dendrimer conjugates. *Chem. Commun.* **52**, 10357–10360.
32. Dvir, H., I. Silman, M. Harel, T. L. Rosenberry and J. L. Sussman (2010) Acetylcholinesterase: From 3D structure to function. *Chem.-Biol. Interact.* **187**, 10–22.
33. Singh, M., M. Kaur, H. Kukreja, R. Chugh, O. Silakari and D. Singh (2013) Acetylcholinesterase inhibitors as Alzheimer therapy: From nerve toxins to neuroprotection. *Eur. J. Med. Chem.* **70**, 165–188.
34. Worek, F., H. Thiermann and T. Wille (2020) Organophosphorus compounds and oximes: A critical review. *Arch. Toxicol.* **94**, 2275–2292.
35. Mercey, G., T. Verdelet, J. Renou, M. Kliachyna, R. Baati, F. Nachon, L. Jean and P.-Y. Renard (2012) Reactivators of acetylcholinesterase inhibited by organophosphorus nerve agents. *Acc. Chem. Res.* **45**, 756–766.
36. Franklin, M. C., M. J. Rudolph, C. Ginter, M. S. Cassidy and J. Cheung (2016) Structures of paraoxon-inhibited human acetylcholinesterase reveal perturbations of the acyl loop and the dimer interface. *Proteins: Struct. Funct. Bioinf.* **84**, 1246–1256.
37. Wong, L., Z. Radić, R. J. M. Brüggemann, N. Hosea, H. A. Berman and P. Taylor (2000) Mechanism of oxime reactivation of acetylcholinesterase analyzed by chirality and mutagenesis. *Biochemistry* **39**, 5750–5757.
38. Farizatto, K. L. G., M. F. Almeida, R. T. Long and B. A. Bahr (2019) Early synaptic alterations and selective adhesion signaling in hippocampal dendritic zones following organophosphate exposure. *Sci. Rep.* **9**, 6532.
39. Tang, S., P. T. Wong, J. Cannon, K. Yang, S. Bowden, S. Bhattacharjee, J. J. O'Konek and S. K. Choi (2019) Hydrophilic scaffolds of oxime as the potent catalytic inactivator of reactive organophosphate. *Chem.-Biol. Interact.* **297**, 67–79.
40. Cannon, J., S. Tang, K. Yang, R. Harrison and S. K. Choi (2021) Dual acting oximes designed for therapeutic decontamination of reactive organophosphates via catalytic inactivation and acetylcholinesterase reactivation. *RSC Med. Chem.* **12**, 1592–1603.
41. Kawaguchi, M., T. Tani, R. Hombu, N. Ieda and H. Nakagawa (2018) Development and cellular application of visible-light-controllable HNO releasers based on caged Piloty's acid. *Chem. Commun.* **54**, 10371–10374.
42. Tang, S., J. Cannon, K. Yang, M. F. Krummel, J. R. Baker and S. K. Choi (2020) Spacer-mediated control of coumarin uncaging for photocaged thymidine. *J. Org. Chem.* **85**, 2945–2955.
43. Braslavsky, S. E. (2007) Glossary of terms used in photochemistry, 3rd edition (IUPAC Recommendations 2006). *Pure Appl. Chem.* **79**, 293–465.
44. Ellman, G. L., K. D. Courtney, V. Andres Jr and R. M. Featherstone (1961) A new and rapid colorimetric determination of acetylcholinesterase activity. *Biochem. Pharmacol.* **7**, 88–95.
45. de Koning, M. C., G. Horn, F. Worek and M. van Grol (2018) Discovery of a potent non-oxime reactivator of nerve agent inhibited human acetylcholinesterase. *Eur. J. Med. Chem.* **157**, 151–160.
46. Worek, F., H. Thiermann, L. Szinicz and P. Eyer (2004) Kinetic analysis of interactions between human acetylcholinesterase, structurally different organophosphorus compounds and oximes. *Biochem. Pharmacol.* **68**, 2237–2248.
47. Sit, R. K., Z. Radić, V. Gerardi, L. Zhang, E. Garcia, M. Katalinić, G. Amitai, Z. Kovarik, V. V. Fokin, K. B. Sharpless and P. Taylor (2011) New structural scaffolds for centrally acting oxime reactivators of phosphylated cholinesterases. *J. Biol. Chem.* **286**, 19422–19430.
48. Kurata, M., M. Hiyama, T. Narimatsu, Y. Hazama, T. Ito, Y. Hayamizu, X. Qiu, F. M. Winnik and H. Akiyama (2018) Synthesis and quantitative characterization of coumarin-caged D-luciferin. *J. Photochem. Photobiol. B* **189**, 81–86.
49. Imoto, T., A. Kawase, M. Minoshima, T. Yokoyama, H. Bito and K. Kikuchi (2020) Photolytic release of a caged inhibitor of an endogenous transcription factor enables optochemical control of CREB-mediated gene expression. *Org. Lett.* **22**, 22–25.
50. Karamtzioti, P., A. Papastergiou, J. G. Stefanakis, A. E. Koumbis, I. Anastasiou, M. Koffa and K. C. Fylaktakidou (2015) O-Benzoyl pyridine aldoxime and amidoxime derivatives: Novel efficient DNA photo-cleavage agents. *Med. Chem. Comm.* **6**, 719–726.
51. Schoenleber, R. O. and B. Giese (2003) Photochemical release of amines by C, N-bond cleavage. *Synlett* **4**, 501–504.
52. Asad, N., D. Deodato, X. Lan, M. B. Widegren, D. L. Phillips, L. Du and T. M. Dore (2017) Photochemical activation of tertiary amines for applications in studying cell physiology. *J. Am. Chem. Soc.* **139**, 12591–12600.
53. Asad, N., D. E. McLain, A. F. Condon, S. Gore, S. E. Hampton, S. Vijay, J. T. Williams and T. M. Dore (2020) Photoactivatable dopamine and sulpiride to explore the function of dopaminergic neurons and circuits. *ACS Chem. Neurosci.* **11**, 939–951.
54. Tang, X.-J., Y. Wu, R. Zhao, X. Kou, Z. Dong, W. Zhou, Z. Zhang, W. Tan and X. Fang (2020) Photorelease of pyridines using a metal-free Photoremovable Protecting Group. *Angew. Chem. Int. Ed.* **59**, 18386–18389.
55. Cürten, B., P. H. M. Kullmann, M. E. Bier, K. Kandler and B. F. Schmidt (2005) Synthesis, photophysical, photochemical and biological properties of caged GABA, 4-[[(2H-1-Benzopyran-2-one-7-amino-4-methoxy) carbonyl] amino] butanoic acid. *Photochem. Photobiol.* **81**, 641–648.
56. Porel, M., C.-H. Chuang, C. Burda and V. Ramamurthy (2012) Ultrafast photoinduced electron transfer between an incarcerated donor and a free acceptor in aqueous solution. *J. Am. Chem. Soc.* **134**, 14718–14721.
57. Worek, F., G. Reiter, P. Eyer and L. Szinicz (2002) Reactivation kinetics of acetylcholinesterase from different species inhibited by highly toxic organophosphates. *Arch. Toxicol.* **76**, 523–529.
58. Petroianu, G. A., K. Arafat, S. M. Nurulain, K. Kuča and J. Kassa (2007) In vitro oxime reactivation of red blood cell acetylcholinesterase inhibited by methyl-paraoxon. *J. Appl. Toxicol.* **27**, 168–175.
59. Momotake, A., N. Lindegger, E. Niggli, R. J. Barsotti and G. C. R. Ellis-Davies (2006) The nitrodibenzofuran chromophore: A new caging group for ultra-efficient photolysis in living cells. *Nat. Methods* **3**, 35–40.
60. Jones, A. L., J. Jiang and K. S. Schanze (2020) Excitation-wavelength-dependent photoinduced electron transfer in a π-conjugated diblock oligomer. *J. Am. Chem. Soc.* **142**, 12658–12668.